Deep-Sea Research II 58 (2011) 1052–1061

Contents lists available at ScienceDirect

Deep-Sea Research II

journal homepage: www.elsevier.com/locate/dsr2

Bio-optical properties of Antarctic pack ice in the early austral spring

Christian H. Fritsen [a,*], Eric D. Wirthlin [a], Diane K. Momberg [a], Michael J. Lewis [b], Stephen F. Ackley [b]

[a] Division of Earth and Ecosystem Sciences, Desert Research Institute, Reno, NV, USA
[b] Geological Sciences Department, University of Texas at San Antonio, San Antonio, TX, USA

ARTICLE INFO

Article history:
Received 20 October 2010
Accepted 20 October 2010
Available online 18 November 2010

Keywords:
Algae
Sea ice
Optics
PAR
Snow
Ultraviolet radiation

ABSTRACT

Pack ice in the Bellingshausen Sea contained moderate to high stocks of microalgal biomass (3–10 mg Chl *a* m^{-2}) spanning the range of general sea-ice microalgal microhabitats (e.g., bottom, interior and surface) during the International Polar Year (IPY) Sea Ice Mass Balance in the Antarctic (SIMBA) studies. Measurements of irradiance above and beneath the ice as well as optical properties of the microalgae therein demonstrated that absorption of photosynthetically active radiation (PAR) by particulates (microalgae and detritus) had a substantial influence on attenuation of PAR and irradiance transmission in areas with moderate snow covers (0.2–0.3 m) and more moderate effects in areas with low snow cover. Particulates contributed an estimated 25 to 90% of the attenuation coefficients for the first-year sea ice at wavelengths less than 500 nm. Strong ultraviolet radiation (UVR) absorption by particulates was prevalent in the ice habitats where solar radiation was highest—with absorption coefficients by ice algae often being as large as that of the sea ice. Strong UVR-absorption features were associated with an abundance of dinoflagellates and a general lack of diatoms—perhaps suggesting UVR may be influencing the structure of some parts of the sea-ice microbial communities in the pack ice during spring. We also evaluated the time-varying changes in the spectra of under-ice irradiances in the austral spring and showed dynamics associated with changes that could be attributed to coupled changes in the ice thickness (mass balance) and microalgal biomass. All results are indicative of radiation-induced changes in the absorption properties of the pack ice and highlight the non-linear, time-varying, bio-physical interactions operating within the Antarctic pack ice ecosystem.

© 2010 Elsevier Ltd. All rights reserved.

1. Introduction

Disposition of solar radiation in the oceans influences key physical, chemical and biotic processes (e.g., biological productivity, animal behaviors, thermodynamics and mixing, and chemical reactions) that help shape almost all upper oceanic system properties. In ice-covered polar waters the temporal and spatial variations in the solar radiation entering the ocean are mostly determined by diurnal and seasonal variations in incident irradiances, the amount and types of ice and snow cover and their inherent optical properties. It has been well established through quantitative radiative transfer studies (Perovich et al., 1986) and modeling (Perovich, 1990; Perovich and Grenfell, 1982) that snow cover (and its attributes) is perhaps the most optically influential geophysical feature because of its high attenuation of photons across all wavelengths of ultraviolet and visible light (with attenuation coefficients ranging from 5 to 30 m^{-1} in ultraviolet and visible wavelengths (Perovich, 1990; Perovich et al., 1993; Warren, 1982). In addition to snow, variations in radiation transfer in and through sea ice are determined by crystalline structure, gas and brine inclusions of the sea ice itself as well as the time and spatially variable content of particulates and dissolved organic matter and their inherent optical properties (Arrigo et al., 1991; Fritsen et al., 1992; Mundy et al., 2007; Palmisano et al., 1987; Perovich et al., 1986).

Interactions among dynamic air temperatures, ocean heat fluxes, precipitation and currents within the pack-ice realms of the Antarctic occur in a myriad of combinations that create a wide range of ice types with diverse and dynamic bottom, interior, surface ice and snow habitats supporting productive microalgal communities (Fritsen and Sullivan, 1999; Garrison et al., 1986; Horner, 1980; Meguro, 1962; Thomas and Dieckmann, 2002). Microalgal communities in land-fast ice of the Arctic and Antarctic have been shown to have a large contribution to the attenuation of visible radiation through the ice and influence the spectral characteristics of visible light passing through the ice as blooms develop (Arrigo et al., 1991; Palmisano et al., 1987; Perovich et al., 1993; Smith et al., 1988). Moreover, modeling studies have demonstrated that microalgae can often be the primary visible light-energy-absorbing material in the ice that can influence the localized heating and melting process (Fritsen et al., 1992; Zeebe et al., 1996).

Snow cover and sea ice are thought to be the primary modulators of ultraviolet radiation transfer into areas of the ocean that

* Corresponding author. Tel.: +775 673 7487; fax: +775 673 7485.
E-mail address: chris.fritsen@dri.edu (C.H. Fritsen).

0967-0645/$ - see front matter © 2010 Elsevier Ltd. All rights reserved.
doi:10.1016/j.dsr2.2010.10.028

are affected by stratospheric ozone depletion (Perovich, 1993) due to their relatively large attenuation coefficients in the ultraviolet wavelengths (10–30 m^{-1} for snow and 1–10 m^{-1} for sea ice). The presence of microsporine-like amino acids (MAAs) in sea-ice microalgae (Karentz, 1994) and CDOM in sea ice that absorbs UVR (Norman et al., 2011) also implies that UVR transmission may be determined, in part, by sea-ice biota and biological processes. Because sea-ice biota and organic matter are released into the water column upon melting in the spring and summer, their UVR and visible light absorbing properties are likely to be primary determinants of the nature of the light field in the water column as the ocean becomes ice-free.

The optical properties and contribution of ice-algae and particulate matter in determining the fate of solar radiation (both visible and ultraviolet) within the pack ice of the Southern Ocean remain largely undocumented despite general recognition of the potential for microalgae in affecting radiative transfer and key processes such as primary production and ice thermodynamics. To help achieve the overall aim of evaluating the variation in sea-ice algal biomass and its effects on radiation transfer within the Antarctic pack ice we conducted an assessment of spectral irradiances above and below a range of different types of first-year sea ice located at the Sea Ice Mass Balance (SIMBA) study area in the Bellingshausen Sea during the late-winter to early-spring (October–November) of 2007. We collected particulate matter from within the ice to evaluate the spectral absorption properties of the algae and their effects upon the absorption and transmission of radiation. A time-series of under-ice spectral irradiances was collected at one of the sites in conjunction with ice and snow mass-balance instrumentation (Lewis et al., 2011) to determine if light transmission through the ice could be linked to the time-varying geophysical and biological processes operating within the coupled physical-chemical-biotic system.

2. Methods

Optical measurements and ice core collections were undertaken at three separate sites during the IPY-SIMBA operations. These sites were in relatively close proximity (50–75 m distant) of the "Brussels" and "Liege" sampling/study sites as described by Lewis et al. (2011) and another site was near the ship. In brief, all of these sites were first-year ice ranging in thickness from 0.5 to 1.3 m. The ice at the Brussels site ranged between ~0.5 to 0.65 m, with a relatively thin snow cover (0.02–0.15 m thick) and relatively little deformation. The study location near the ship had thicker ice (0.6–0.8 m) with a thicker snow cover of 0.12 to 0.2 m; the sampling site at the Liege location had even more snow (0.25–0.3 m) and thicker ice (up to 1.2 m) than the other two sites. Ice and snow thickness in conjunction with deformation were all indicative that the ice at the latter locations was older than the thinner, first-year ice at the Brussels location.

Ice sampling and irradiance measurements were undertaken at two sites located approximately 30 m apart on October 6 near the Brussels study location. One location corresponded to a site approximately 10 m distant from the Ice Mass Balance Buoy (IMB) as described by Lewis et al. (2011). Sampling and measurements were repeated on October 16 at the Brussels site. Sampling and measurements occurred near the ship on October 5 and on October 10 at the Liege location.

Spectral irradiances were measured with an Ocean Optics USB2000 spectrophotometer equipped with a 20-m Vis-NIR 500 optical fiber tipped with a flat cosine collector. Surface incident and upwelling irradiance measures were obtained immediately prior to and after under-ice irradiance measurements. Surface readings of PAR (using a QSL-100) were concurrently measured during surface and under-ice irradiance measurements so all measurements had reference readings that could be used to account for changes in the incident light during the measurements.

Under-ice irradiance measurements were accomplished by deploying the tip of the fiber on an articulated arm deployed through a 0.10-m diameter hole in the ice that was created by obtaining an ice core (using a Mark II ice coring system; Kovacs Enterprises). The tip of the articulated arm was 2.5 m distance from the hole when the tip was raised to be just under the bottom of the ice. Placement of the tip under the ice was accomplished by raising the arm until it gently touched the bottom of the ice and was then slightly lowered (approximately 0.01–0.02 m) by the person holding the apparatus. The arm was manually held in a level position during under-ice irradiance measures and checked with a bubble level. The USB2000 system's time integrations were decreased for above-ice measurements such that irradiance readings were obtained that did not saturate the sensors. Time integrations were increased for under-ice readings to obtain measurements significantly above the dark voltages (according to the manufacture's recommendations). All readings were normalized to a constant integration time. Under-ice irradiance measures were increased by a constant factor of 0.3 to account for the effect of immersing the cosine sensor in water.

Small-scale (meter scale) variations in the under-ice spectral irradiance fields were evaluated by rotating the articulated arm through a 180^{o} arc and measuring the under-ice irradiances at five equidistant locations along this arc (specifically at the 0, 45, 90, 135 and 180° angles along the arc). At each location along the arc two under-ice irradiance readings were obtained within a span of 1-2 minutes. After all irradiance measurements were taken, we measured the snow depth at each location along the arc (with a metal meter stick) 5 to 10 separate times within an area approximately 0.3 m in diameter.

Ice cores were obtained at each site with a 0.1 m diameter core barrel, immediately sectioned and placed in 4 L widemouth HDPE jars for transport back to the ship. A cold (0–2 °C), filter-sterilized solution of 240 ppt NaCl was added to the core sections (0.1-0.2 m) to yield a final salinity upon melting of 36 psu– and thus minimize hypo-osmotic bursting of the biota during the melting process (Garrison and Buck, 1986). Melting of ice cores was accomplished at 2-3 °C and generally occurred over 6 to 8 hours. Cores were nominally obtained from ice at the point where the articulated arm was inserted through the ice at each site. An additional core was taken from the Ship site on October 5 and two more from the Brussels site on October 6 and 16. The bottom 0.03 m from these latter cores were subsampled to examine and measure biomass concentrations in the bottom ice layer that was commonly observed at this site. Sampling of the ice at the Liege location was kept to a minimum due to resource constraints and the desire to keep the site preserved for ongoing time-series studies by other colleagues.

Particulates in the ice melt water were gently filtered (at less than 7 mbar in subdued light) onto Whatman® glass fiber filters (GF/F), which were then treated to derive total particulate absorption ($a_p(\lambda)$), absorption by detritus ($a_d(\lambda)$) and microalgae ($a_a^*(\lambda)$) using methanol extraction (Kishino et al., 1985) and applying path-length amplification corrections for the filter-pad method (Tassan and Ferrari, 1995). Analysis was completed using a Lambda-18 and a CARY 300 spectrophotometer (each equipped with a Labsphere integrating sphere). Chlorophyll *a* (Chl *a*) concentrations in the ice-core melt water was determined by filtering melt water through GF/Fs, extracting filters and measuring Chl *a* in the extract according to the EPA 445 method using a Turner 10 AU fluorometer standardized with pure *Anacystis* Chl *a* (Sigma).

Aliquots of the ice-core melt water were preserved with glutaraldehyde (Sigma G6403; 0.5% final concentration), kept chilled at 0-2 °C and shipped back to the Desert Research Institute (DRI) for microscopic analysis. Samples were settled in Utermöhl-settling chambers (minimum settling time of 24 hours) and settled

biota were enumerated using a combination of Nomarski and Epifluorescence microscopy (Olympus BX60 at 100x, 200x magnification) in concert with phase contrast microscopy (Olympus CKX41 400x). Cell biovolumes were calculated using geometric shapes and volume calculations (Hillebrand et al., 1999).

An under-ice Satlantic radiometer (model OCR-504) with four spectral bands (442, 455, 490 and 555 nm) was deployed beneath the ice near the Brussels location on an articulated arm made of PVC. The radiometer was deployed at a final depth of approximately 2.0 m and the PVC pole was leveled and frozen into the ice on October 1. The radiometer pole was located approximately 2 m distant from the remainder of the integrated ice mass balance buoy (Lewis et al., 2011). Data from the integrated station were relayed at 2-hr intervals through the ARGOS satellite from October 2 to November 26, 2007. This time series provided an extension of the temporal information past October 23 when the ship departed the location.

3. Results

3.1. Under-ice irradiances

Peak transmission (under-ice irradiance normalized to surface irradiance) was at 545-550 nm at the Brussels location, 555–560 nm at the site by the ship, and 560 nm at the Liege study site (Fig. 1). The transmittance spectra at the Liege site displayed more spectral dependence compared to the other sites (Fig. 1C). Much of the inter-site variations in transmission were readily explained by variations in the snow thickness. For instance, at the Ship and Brussels sites on October 5 and 6 the transmittance spectra at positions with 0.19 and 0.03 m snow varied by more than three-fold at 400–550 nm.

3.2. Attenuation coefficients

Difference spectra and changes in snow depth at the Brussels and Ship sites were used to calculate apparent snow attenuation coefficients, $K_{snw}(\lambda)$ (Fritsen et al., 1992). These K_{snw} (λ) values show spectral variation and values (12–25 m^{-1}; Fig. 2A) that are well within the range of $K_{snw}(\lambda)$ values previously reported for

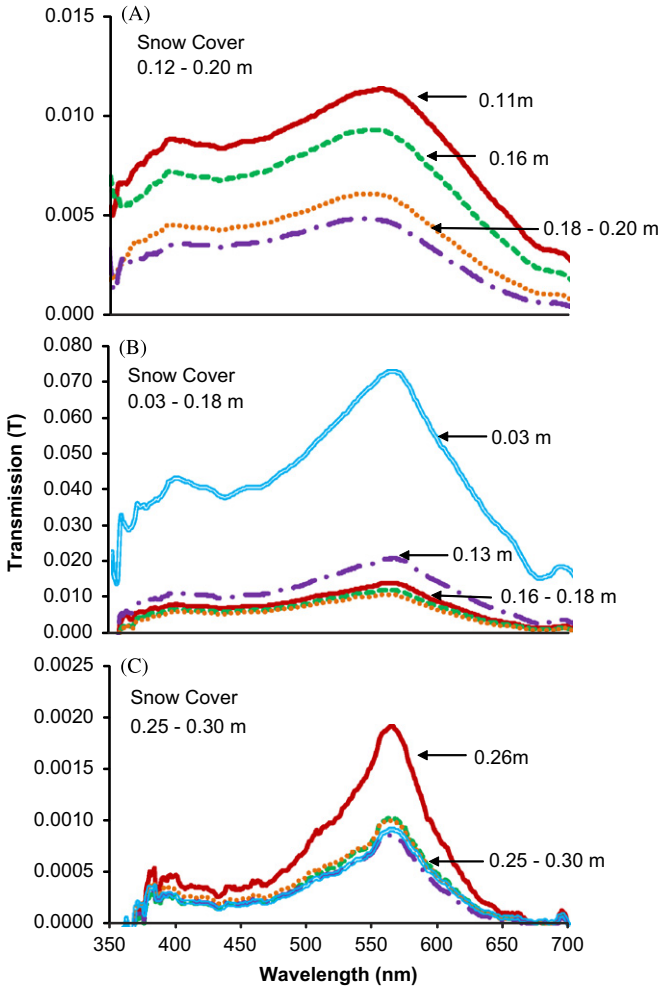

Fig. 1. Transmission (T) spectra derived from the under-ice irradiance normalized to surface-irradiance measurements collected at five different positions (represented by different different graphs) from a central location at each of the study sites Brussels (A), Ship (B), and Liege (C).

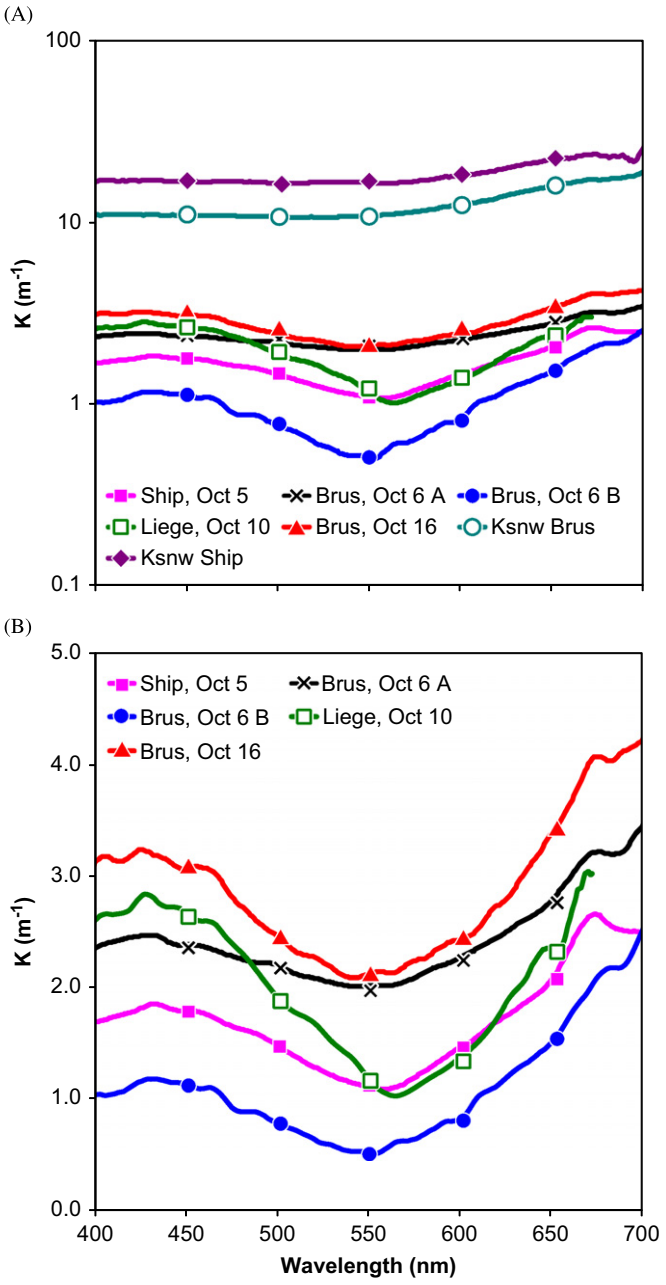

Fig. 2. Calculated spectral attenuation coefficients for the snow and ice covers at the study locations. Panel A is log scale on the y-axis and includes the snow attenuation coefficients (K_{snw}; see text for details) while panel B is normal scale and only includes the ice coefficients in order to show maxima and minima in the spectra.

snow (Mundy et al., 2005; Perovich, 1990; Perovich and Grenfell, 1982; Perovich et al., 1986).

After accounting for albedo and attenuation of downwelling irradiances through the snow covers at the respective locations, the bulk downwelling attenuation coefficients of the ice ($K_{ice}(\lambda)$) at the different sites were estimated assuming simple exponential attenuation of downwelling irradiances (Fritsen et al., 1992; Perovich et al., 1993). The resultant spectral attenuation coefficients varied by an average of 3- to 5-fold among the different locations ranging between 1–3 m^{-1} at 448 nm, 0.5–2.25 m^{-1} at 550 nm and 2.0–3.9 m^{-1} at 660 nm (Figs. 2A and 2B). All sites had spectral attenuation coefficients with a minima that fell within the range of 540–560 nm wavelengths and two peaks on either side of this minima, with one peak occurring within the broad window of 440–450 nm and the other at approximately 660 nm (Fig. 2B).

3.3. Particulate absorption spectra, biomass and microalgal taxa

Particulate absorption spectra ($a_p(\lambda)$) from all of the sampling locations (Figs. 3A, 4A, and 5A) had attributes in the visible wavelengths that were indicative of pigmented algal cells (peaks or inflections at 400–450 and 674 nm) and detritus (monotonic exponential increase in absorbance as λ decreases). Absorption features in $a_p(\lambda)$ from all locations and most depths in the ice cores were indicative of algae being the primary light-absorption particulate material in the ice. The only exception to this apparent dominance was in the bottom sections of ice from the Liege location (at 1.0 to 1.18 m in the ice core) where a_p values were low (e.g., only 0.05 m^{-1} at 400 nm) as were Chl *a* concentrations (1–2 mg Chl *a* m^{-3}; Fig. 5) and spectra had exponentially decreasing absorption with increasing wavelength that is typical for detritus absorption (Arrigo et al., 1998; Ferrari and Tassan, 1996; Fritsen et al., 1992).

Absorption peaks in the ultraviolet wavelengths were readily measured in particulates from all locations. Absorption peaks located at ~325 nm were as high as 6.0 m^{-1} (Fig. 4A). More typically, absorption at 325 nm ranged from 0.5 to 3.0 m^{-1}. These high values were measured at all locations—although there was an apparent trend for the UVR absorption feature to be more pronounced in the ice particulates near the surface of the ice cores (most noticeable at Liege; Fig. 5A).

The methanol-extractable absorption spectra also showed this prominent UVR absorption feature at 325 nm along with absorption features attributable to the microalgal pigments (Figs. 3B, 4B

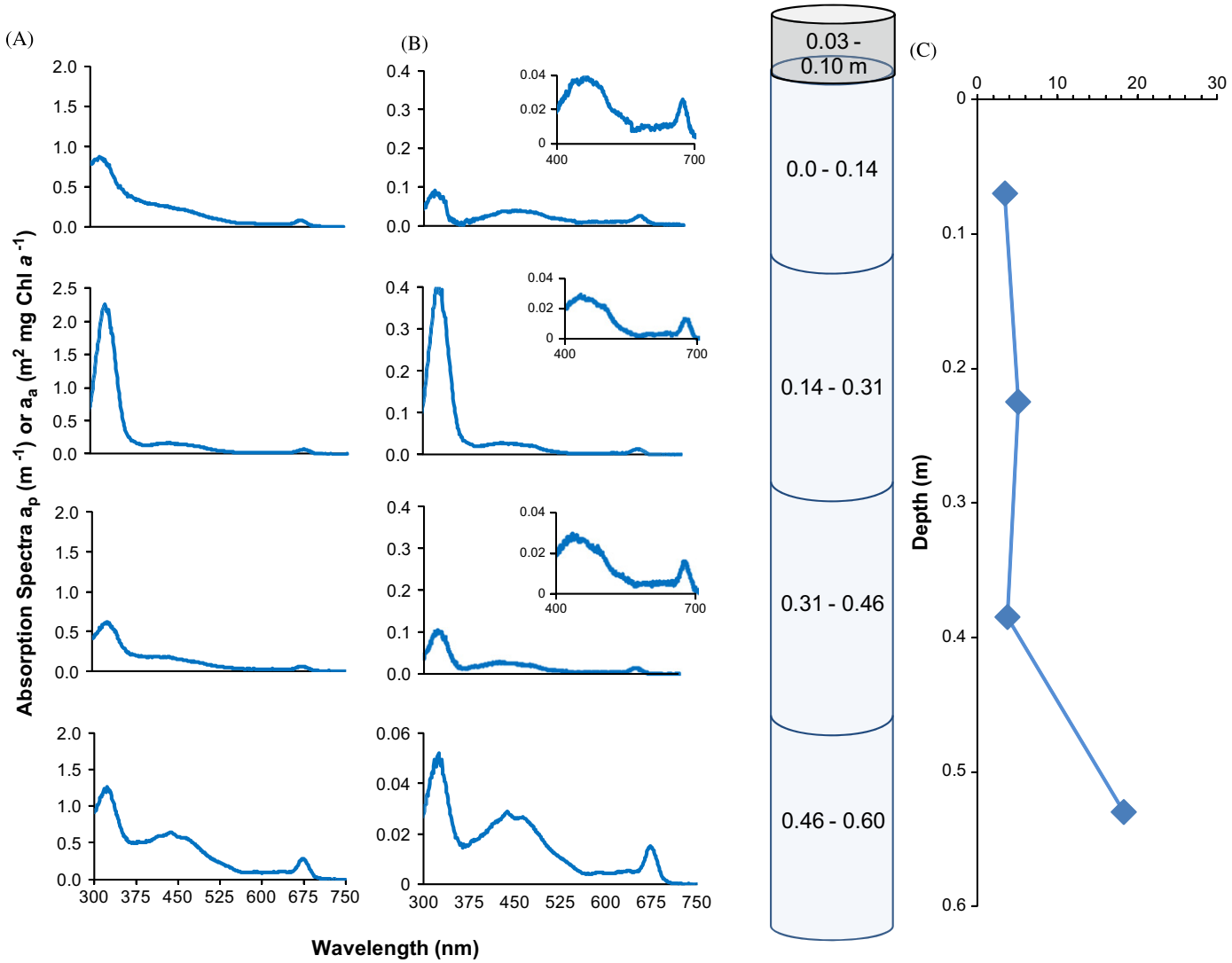

Fig. 3. (A) Particulate absorption spectra (m^{-1}) and (B) biomass specific algal absorption spectra (m^2 mg Chl a^{-1}) for the discrete sections of the ice core obtained from the "Brussels" study site on October 16, 2007. Insets are to show absorption features characteristic of algal pigments from 400 to 700 nm not clearly seen on the same scale as the UV absorption peak. (C) Chlorophyll *a* concentrations for each corresponding core section. Snow cover at the time of collection of the core was 0.03 to 0.10 m and is denoted by grey section at the top of the illustrated core.

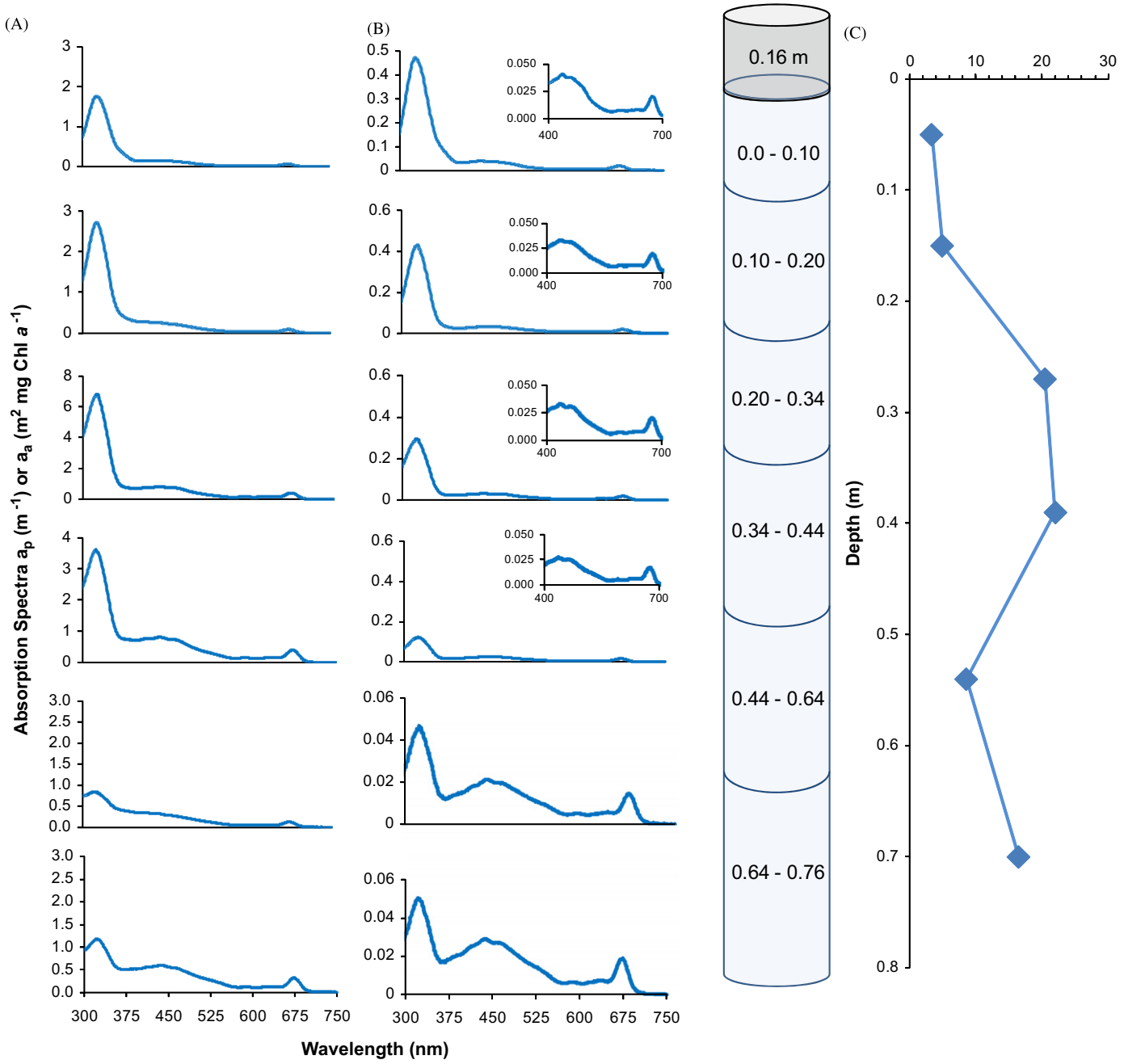

Fig. 4. (A) Particulate absorption spectra (m^{-1}) and (B) biomass specific algal absorption spectra (m^2 mg Chl a^{-1}) for the discrete sections of ice core 2 (Table 1) obtained from the "Ship" study site on October 5, 2007. Insets are to show absorption features characteristic of algal pigments from 400 to 700 nm not clearly seen on the same scale as the UV absorption peak. (C) Chlorophyll *a* concentrations for each corresponding core section. Snow cover at the time of collection of the core was 0.16 m and is denoted by grey section at the top of the illustrated core.

and 5B). The ratio of $a_a^*(325)$ to $a_a^*(444)$ (Fig. 6) showed a larger range in values near the surface of the cores and was much reduced at depths greater than ~0.50 m. The $a_a^*(325)$ peaks were negligible in particulates in the "older" first-year sea ice at the Liege location, even in the 0.25 to 0.45-m section with a modestly high Chl *a* concentration (18.5 mg Chl *a* m^{-3}; Fig. 5).

Profiles of Chl *a* concentration indicated that the majority of the microalgal biomass within the ice at the Ship and Liege site was located within the ice interior (with peak concentrations being measured between 20 to 30 mg Chl *a* m^{-3} in the upper 0.4 m of the ice). Concentrations of Chl *a* at the Brussels site were highest (40–50 mg Chl *a* m^{-3}) near the bottom of the ice (Figs. 3–5C). Integrated standing stocks of Chl *a* varied between 3.1 to 9.97 mg Chl *a* m^{-2} among all sites (Table 1).

Microalgal assemblages were dominated by diatoms and gymnodinoid dinoflagellates at the Brussels site; a mix of gymnodinoid dinoflagellates, diatoms, and *Phaeocystis* at the Ship site; and diatoms at the Liege site. A trend common among all sites was decreasing Gymnodinoid dinoflagellate abundance and biovolume with increasing depth in the ice. The reverse trend was observed for diatoms.

The community composition in samples from the surface and interior sections of the ice cores at the Brussels site consisted primarily of Gymnodinoid dinoflagellates (87 and 97% of abundance and

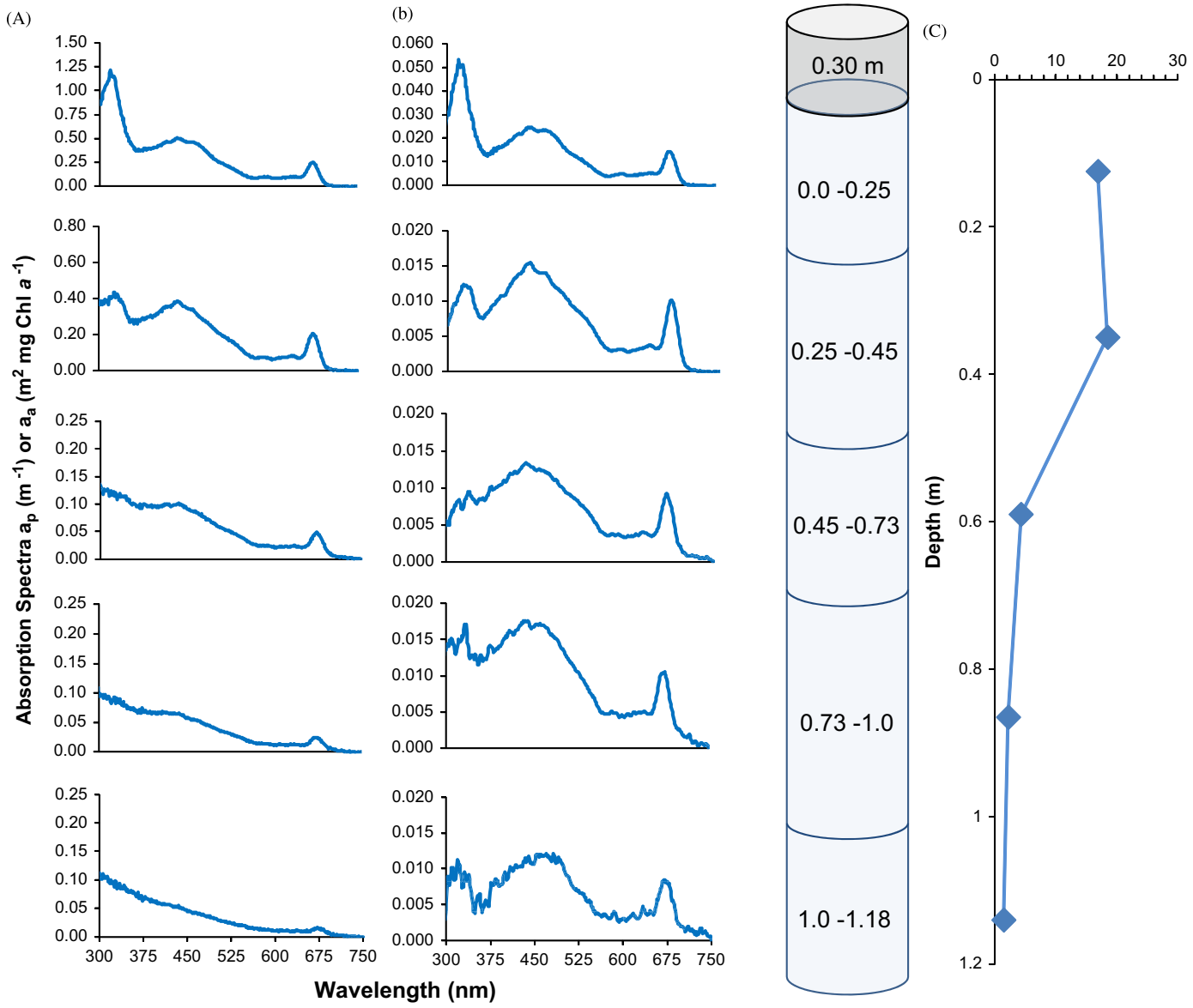

Fig. 5. (A) Particulate absorption spectra (m^{-1}) and (B) biomass-specific algal absorption spectra (m^2 mg Chl a^{-1}) for the discrete sections of the ice core obtained from the "Liege" study site on October 10, 2007. (C) Chlorophyll *a* concentrations for each corresponding core section. Snow cover at the time of collection of the core was 0.30 m and is denoted by grey section at the top of the illustrated core.

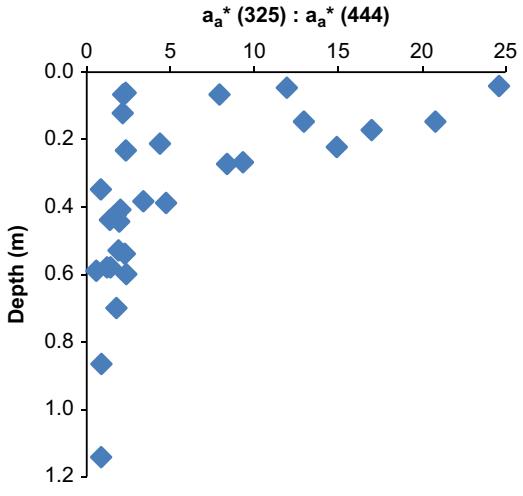

Fig. 6. Ratio of $a_a^*(325)$: $a_a^*(444)$ plotted against the depth in the ice core from which particulate samples were collected.

biovolume, respectively). In contrast, bottom sections of these ice cores were numerically dominated by *Fragilariopsis* sp. (81%), yet biovolume dominance was divided among Gymnodinoid dinoflagellates, *Corethron*, and *Rhizosolenia* (32%, 30%, and 16% of biovolume, respectively; Table 1).

Dominance within the communities throughout the length of the ice core at the site near the ship was shared among a greater number of genera than either Liege or Brussels: *Fragilariopsis* and *Phaeocystis* (39% and 28% abundance, respectively), Gymnodinoid dinoflagellates, ciliates, *Banquisia*, *Pseudo-nitzschia* and *Entomoneis* (35, 14, 11, 11, and 9% of biovolume, respectively; Table 1).

Microalgae within the Liege site consisted primarily of diatoms (accounting for $>80\%$ of core abundance and biovolume). The diatom genera consisted of *Fragilariopsis* sp. (80% of abundance) and the larger genera *Rhizosolenia*, *Corethron* and *Entomoneis* (36, 17, and 12% biovolume, respectively). Gymnodinoid dinoflagellates were also present, but at reduced relative abundances and biovolumes (3–10% of abundance and 2–25% of biovolume between near-surface and near-bottom ice) compared to the other study locations.

Table 1
Summary of sampling dates, locations, and corresponding sea-ice environment parameters: thickness (H) of ice and snow, chlorophyll a as depth-integrated (Chl *a*) and weighted average (< Chl *a* >) and depth-integrated algal community composition by class. Bac, Bacillariophyceae; Din, Dinophyceae; Het, Heterotrichea; Hap, Haptophyceae.

Site	Date	H_{ice} (m)	Avg. H_{snow} (m)	Chla (mg m^{-2})	< Chla > (mg m^{-3})	Community Composition							
						% Abundance				% Biovolume			
						Bac	Din	Het	Hap	Bac	Din	Het	Hap
Brussels	10/1/2007	0.65	-	4.57	7.03	66	33	1	0	44	56	0	0
Ship	10/5/2007	0.76	0.16	9.56	12.57	22	6	8	63	43	41	9	6
Ship	10/5/2007	0.68	0.03	6.08	8.94	58	11	19	13	52	33	15	1
Brussels	10/6/2007	0.54	0.17	3.14	5.81	-	-	-	-	-	-	-	-
Brussels	10/6/2007	0.55	0.03	3.87	7.04	-	-	-	-	-	-	-	-
Brussels[a]	10/6/2007	0.04	-	1.50	49.91	-	-	-	-	-	-	-	-
Liege	10/10/2007	1.18	0.28	9.97	8.45	83	3	12	1	82	8	10	0
Brussels	10/16/2007	0.60	-	4.49	7.48	-	-	-	-	-	-	-	-
Brussels[a]	10/16/2007	0.03	-	1.62	40.43	90	10	0	0	84	16	0	0

[a] Only the bottom section of these cores were analyzed.

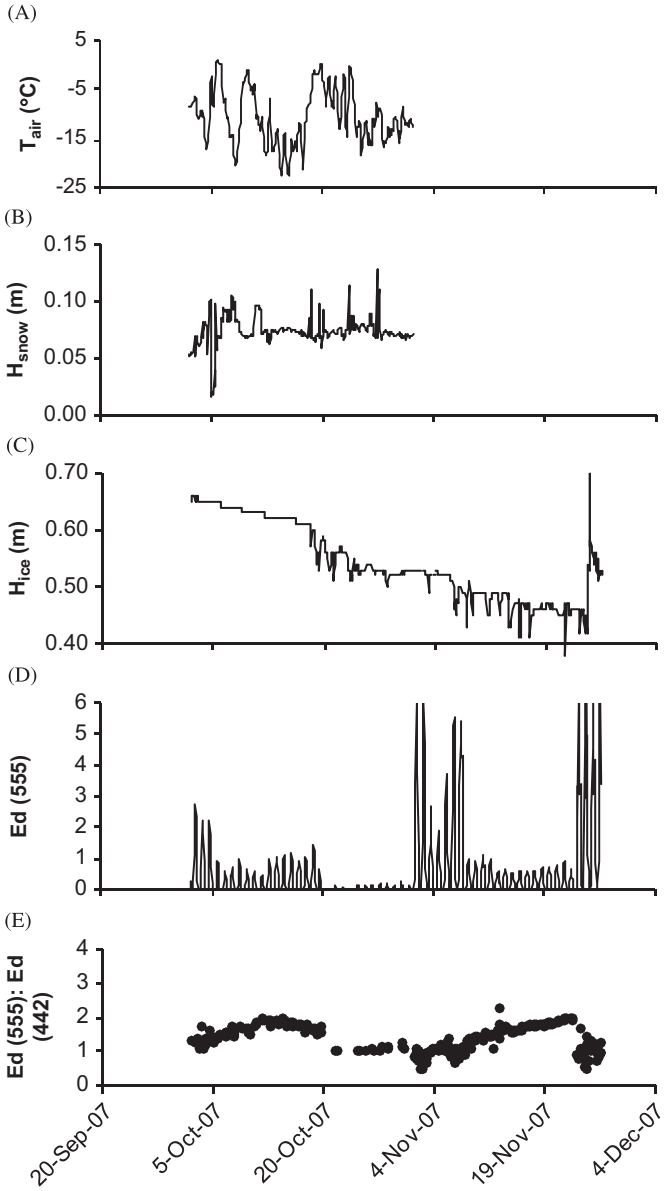

Fig. 7. Time series of air temperature, T_{air} (A), snow thickness, H_{snow} (B), ice thickness, H_{ice} (C), under-ice irradiance at 555 nm, E_d555 (D) and the ratio of under-ice irradiances at 555 and 442 nm (E).

3.4. Temporal dynamics

The ice-mass balance buoy recorded dynamic thermal, mass and radiative processes near the Brussels sampling location. Air temperatures fluctuated from 0 to −20 °C during October (Fig. 7A). Snow thickness, recorded by the acoustic sensor, only fluctuated between 0.06 and 0.1 m. However, the snow pinger was located 2 to 3 m distant from the radiometer location and was not necessarily recording conditions that were representative of the snow cover that influenced the radiometer during the study. In fact, on October 19, 0.4 m of snow was manually recorded above the radiometer when an abrupt wind and warming event occurred and a drift formed above the radiometer location. Coincident with this air temperature increase and drift formation was a rapid loss of approximately 0.05 m of bottom ice (as was recorded as the distance between ice-water interface and the upward facing pinger beneath the ice; Fig. 7C) as well as an abrupt decrease in the under-ice downwelling irradiances (Fig. 7D). The temperature sensors and snow pinger all stopped recording on November 1, for mechanical reasons that cannot be determined (Lewis et al., 2011). The under-ice radiometer began recording much higher under-ice irradiances at this time. Under-ice irradiance again decreased on November 8 and remained low until November 23– three days before all data transmission ceased from the array. The behavior of rapid increases in apparent ice thickness paired with increases in under-ice irradiances just prior to the ending of data transmission is consistent with ice deformation compromising the buoy's integrity and functioning.

The ratio of downwelling under-ice irradiances at 555 and 442 nm (555:442) during midday experienced two distinct periods of gradual increase (from October 2-10, November 1-23). These two periods were intervened by times when the ratio decreased gradually from October 11 to October 31 and abruptly on October 19, November 1 and again on November 23 (Fig. 7E).

4. Discussion

4.1. Transmission and attenuation of PAR

Transmission of PAR in and through the first-year pack ice was generally limited to being less than 1–5% of surface irradiance–even beneath the ice with relatively thin snow covers. The magnitude of the peak wavelengths of PAR transmission was largely determined by the snow cover on the ice due to its high attenuation properties (through both scattering and absorption).

The sea-ice and pigmented microalgal communities imparted additional variations in the attenuation of irradiance.

Spectral attenuation coefficients for the sea ice were highly variable (varying by roughly fivefold). Attenuation coefficients derived at the Brussels site on October 6, with 0.16 m of snow (Fig. 2B), most closely resembled attenuation coefficients for first-year blue ice (Arrigo et al., 1991; Perovich, 1989). Coefficients derived for the other location at the Brussels site on that day and again on October 16 were much larger (with minimum values at approximately 550 nm of 2 m^{-1}) and more closely resembled values for eutectic ice or ice with a white-ice scattering layer (Grenfell, 1983; Perovich and Grenfell, 1982). The magnitude in the values are consistent with the latter two spectra being associated with sites with little insulating snow cover, such that the upper ice column had a small (cm thick) opaque layer near the ice surface. Values for the coefficients at the first Brussels location plus at the Ship and Liege locations are more consistent with those values for warmer first-year ice.

All of the site's attenuation coefficients had peaks at 450–470 and 660 nm that correspond to absorption peaks for algal pigments (e.g., Chl *a*). Spectral attenuation coefficients for ice without the impurities of detritus, algae and dissolved organic matter generally have a convex shape with minima occurring at approximately 480–500 nm with stronger attenuation at wavelengths longer than the minima than those at wavelengths below the minima (this spectral dependence is imparted by the absorption properties of water). None of the attenuation coefficients resembled those of ice without these types of impurities. However, all the spectral attenuation coefficients exhibited monotonic decreases from approximately 650 to 550 nm that closely resembles slopes of attenuation coefficients dominated by that of the sea ice; spectral coefficients at wavelengths less than 550 nm resembled those of a mixture of sea ice, algal pigments, detritus, and DOM.

4.2. Contributions to attenuation

Deconvolution of the bulk attenuation coefficients among the different optical properties of entities in the sea-ice column is difficult given that we did not take measures to derive the brine volume and gas content of the ice (salinity, temperature and density) that would more readily allow the sea-ice optical coefficients to be modeled. However, rough approximations of the contribution of the particulate's absorption to the attenuation coefficients (K_p) can be calculated as the ratio of the absorption to the mean cosine of the light field in a vertical column of the media (in this case sea ice). Assuming a diffuse light field within the ice the mean cosine would be approximately 0.5 to 0.65 (Kirk, 1996) and estimates of the $K_p(440)$ at the different sites would have ranged between 0.3 and 0.8 m^{-1}.

This range in K_p values likely can account for a substantial portion of the broad (400–500 nm) peaks in the sea-ice attenuation coefficients for both the Brussels and Ship sites (Fig. 2B). Again, a precise means of deconvoluting the K_{ice} spectra is not readily attainable. Yet, if an approximation of the base-line K_{ice} values can be inferred from the value of the $K(\lambda)$ minima (at approximately 550 to 560 nm) and the assumption that the K spectra for pure sea ice has a convex shape with a minimum at approximately 450 nm, then the K_p values at these sites could account for approximately 60 to 90% of the total K_{ice} values in the range of approximately 400 to 500 nm. In contrast to the Brussels and Ship sites, the $K_p(440)$ values (estimated from the $a_p(\lambda)$ measured on particulates from the ice core; Fig. 4) would only account for approximately 25% of the $K_{ice}(440)$ coefficient at the Liege site.

CDOM absorption (and attenuation) was not measured during this study and could have better allowed for a full accounting and partitioning of bulk sea-ice attenuation coefficients. CDOM absorption is often similar to detrital absorption (i.e. having a monotonic exponential increase with decreasing wavelength; Kirk, 1996) and CDOM was undoubtedly present in the sea ice during the SIMBA study– as it was present in the pack ice off East Antarctica during the same season and year in ice with even less microalgal biomass (Norman et al., 2011). Thus CDOM would have contributed to the ice attenuation coefficients and would partially help account for the remainder of the difference between $K_p(400–550)$ and $K_{ice}(400–550)$ at all the sites.

The large difference between $K_p(400–550)$ estimates (based on $A_p(\lambda)$; Fig. 4) at the Liege site and the derived attenuation coefficients also may be explained by potential spatial heterogeneity of microalgal biomass (such that biomass in the core was not representative of that in the ice influencing the under-ice readings) or losses of biota and light absorbing materials during sampling or processing. The chlorophyll specific algal absorption coefficients (a_a^*) were similar to those of algae in moderate to low light environments (having $a_a^*(440)$ of approximately 0.03 m^2 mg Chl *a*; Fig. 4). To arrive at K_p values that could more fully account for the differences between $K_p(400–550)$ and $K_{ice}(400–550)$, Chl *a* concentrations would have had to have been roughly 4 times higher (at approximately 40 mg Chl *a* m^{-3}) than the average measured in the ice core (Fig. 4C and Table 1). Given the documented variability in the pack-ice environment (Eicken et al., 1991; Fritsen et al., 2008), potential losses of biomass due to sampling a semi-porous medium (Fritsen, personal observation) and potential osmotic-induced losses of biota (Garrison and Buck, 1986) it is likely that there was more microalgal biomass over the sensor when the under-ice readings were taken at this site than that which was captured in the measurements on the ice core.

The higher microalgal biomass at the Liege site with more snow cover than the other sites is worth noting (Table 1). This relationship is not overly surprising given that the Liege site had thicker ice as well as more snow. Therefore, it is likely that this ice had more time and a relatively warmer environment for microalgal communities to grow and accumulate than the other sites. Several prior studies have demonstrated inverse relationships between snow depth, algal productivity and biomass accumulation (Grossi et al., 1987; Palmisano et al., 1985; Smith et al., 1988). However, this linear relationship has not been documented in Antarctic pack ice (Dieckmann et al., 1998; Garrison et al., 1986). Our results further highlight fundamental differences between the pack ice and land-fast ice regimes of the Antarctic where time, habitat stability, thermal insulation and prior dynamics processes (such as flooding and snow-ice formation) often may be the factors that control productivity and biomass dynamics in the more open ocean setting (Fritsen et al., 2001, 2008; Fritsen and Sullivan, 1997, 1999; Garrison et al., 1986, 2005; Meguro, 1962).

4.3. UVR absorption

In the spring of 2007 the ozone hole began to appear in the late August to September time-frame (http://ozonewatch.gsfc.nasa.gov/) and by October the pack ice that we were sampling was likely exposed to substantial UVR during the prior month (as the seasonal solar radiation increased at these latitudes). The UVR exposures at the time of the study were likely higher in the ice at the Brussels and Ship sites compared to that at the Liege site simply due to the amount of overlying snow.

The presence of major UVR absorbing materials in the ice illustrates the capacity for *in situ* adaptation and productivity by polar microalgae within the Antarctic pack ice habitat. Greater UVR absorption within habitats with relatively small radiation attenuation (i.e. closer to the surface of the ice or with less overlying snow cover) strongly indicates either inherent UVR-photoadapation by the

microbiota or colonization of such sites by biota capable of synthesizing UVR-absorbing compounds.

Prominence of Gymnodinoid dinoflagellates in the interior and upper sea-ice habitats has been noted on several occasions (Stoecker et al., 1992; Stoecker et al., 1997). Their ability for encystment, excystment, and production of compatible solutes for surviving in the highly saline environments have been discussed as potential attributes that may allow their proliferation (Stoecker et al., 1992; Stoecker et al., 1998). The present results further suggest that the ability to synthesize MAAs for UVR protection in pack ice environments (especially those without protective snow covers) may also be a significant factor in structuring the sea-ice biotic communities in the austral spring (Karentz, 1991). Dinoflagellates, and species of *Gymnodinium* in particular, can synthesize MAAs in large concentrations in response to increased radiation (Jeffrey et al., 1999; Neale et al., 1998) as can the species *Phaeocystis antarctica* and *Mesodinium rubrum* (Johnson et al., 2006; Moisan and Mitchell, 2001)— all taxa that were abundant at sampling sites with low or intermediate snow covers.

Diatoms have not been considered extensive producers of MAAs (Jeffrey et al., 1999) and reported concentrations of MAAs in Antarctic bottom-ice communities have been reported as being very low (Ryan et al., 2002). These observations are consistent with obtained a_a^*(UVR) (Fig. 5B) and the distributions of diatoms at the Liege site that had much increased snow cover and, hence, reduced UVR. The distribution of alga-taxa and UVR-absorbing compounds documented in this study raises a question regarding the extent to which the relatively recent creation of the ozone hole (and concomitant increase in austral spring UVR) is imparting a recent UVR-induced change to the Antarctic sea-ice ecosystem.

The production of major UVR-absorbing compounds in ice without UVR-protecting snow covers may be an example whereby biotic-physical feedback interactions highly limit UVR penetration in the water column of ice-covered seas. The potential for UVR screening in marginal ice-edge zones (MIZ) when these ice-algae are released upon the melting of the ice also may confer reduced UVR penetration into the MIZ blooms and perhaps mitigate suspected UVR-induced decreases in productivity (Arrigo et al., 2003; Smith et al., 1992).

4.4. Temporal dynamics

The time series of the radiometer readings at the Brussels location (Fig. 7) clearly shows reductions in under-ice irradiances – that were associated with snow deposition/accumulation events on October 19 (Fig. 7E). Increases in under-ice irradiances on November 1 and again on November 23 may have been due to deformation and perhaps opening of cracks or leads in the ice near the radiometers that allowed more light to reach the sensors.

Changes in the ratio of downwelling irradiances at 555 and 442 nm (E_d555:442) at midday are consistent with changes in the influence of algal biomass on the spectral irradiance field. Simple linear regression of biomass in ice cores and this ratio (as recorded across all study locations with the USB2000 radiometer, N=5) indicates a relationship of 0.6619 (E_d555:442/mg Chl *a* m^{-2}) with 71% of the variability in the ratio being explained by the variation of Chl *a* biomass in the ice cores. When this under-ice irradiance ratio is normalized to the irradiances at those wavelengths (i.e. a normalized difference index; Mundy et al. 2007) 81% of the variation in the ratio was explained by variation in integrated Chl *a*. Thus, the time series of irradiances at the mass balance array at Brussels study site– although dynamic– are likely to be indicative of changes in sea-ice algal biomass.

The gradual increase in the E_d555:442 ratio from October 3 to 11 and again during the first two weeks in November may have been indicative of microalgal growth and a gradual increase in ice-algal biomass. Rapid reduction in the ratio of E_d555:442 in concert with decreasing irradiances and a relatively rapid reduction in ice thickness on October 19 are consistent with the release of microalgal biomass from the bottom side of the ice at this location (where the highest biomass concentrations were found). However, the abrupt decreases in the E_d555:442 ratio in conjunction with abrupt increases in under-ice irradiances are consistent with an increase in the relative proportion of the light that had passed through open water (a crack or lead?) with much less algal influence– as opposed to being indicative of changes in algal biomass in the sea ice. Loss of bottom ice algae in conjunction with ablation of the bottom surface of congelation ice is a commonly reported phenomenon (Fritsen and Sullivan, 1999; Grossi et al., 1984; Smith et al., 1988).

Future deployments of instrumentation packages for monitoring algal biomass remotely may benefit by the inclusion of additional wavelengths (e.g., the wavelengths suggested by Mundy et al. 2007) with radiometers placed above as well as below the ice. Digital imagery, to confirm the status of the under-ice geophysical environment, also would help interpreting these types of remotely produced results. Such transmission of imagery does not need to be cost-prohibitive if images were sent on more intermittent basis (e.g., only once per day).

5. Summary and conclusion

Microalgal absorption contributed substantially to attenuation of irradiances through the first-year pack ice cover during the austral spring in the Bellingshausen Sea (i.e. the SIMBA study area) contributing 25–90% of the attenuation in the violet to blue part of the visible spectrum (i.e. in the range of 400–550 nm). Radiant energy absorption by these particulates can easily be shown to be the primary energy absorption process in the sea ice (Fritsen et al., 1992; Zeebe et al., 1996) and as such, contributes to the physical processes of energy transfer within sea ice. Ice mass-balance instrumentation illustrated dynamics that are indicative of algal growth and loss coupled to the mass balance of the first-year ice. More field studies are needed to determine how algal growth and light-absorption processes affect the mass balance in the pack ice as the seasons progress from the austral spring into austral summer.

Strong UVR absorption appeared in particulates (algae) primarily in the high-light sea-ice habitats, indicating that physical-biological feedback processes creates a complex multifarious ice pack that readily attenuates UVR penetration into the water column during the austral spring when stratospheric ozone depletion is at its greatest. The affects of this material on the water column processes when released remains largely unknown.

Overall, the study provides incremental information regarding bio-physical processes and coupling that is generally lacking for the Antarctic pack ice and its biota. This information confirms and re-enforces assumptions that sea-ice biota substantially contributes to the dynamic bio-physical sea-ice processes operating throughout the Antarctic pack ice. The implications and manifestations of these interactions over large spatial and temporal scales are likely to be under-appreciated.

Acknowledgments

This research was supported by the Desert Research Institute's sabbatical program as well as NSF-Office of Polar Programs grants ANT-0529666 to C. Fritsen and ANT-0703682 to S. Ackley and NASA grant NNX08AQ87G to S. Ackley. Special thanks are also extended to Sharon Stammerjohn and Martin Vancoppenolle for aid in the field, the field and lab technicians within Raytheon Polar Services

Company and the Captain and the crew of the Nathanial B. Palmer. We are also grateful for the service, insight and gracious work provided by the two anonymous reviewers.

References

Arrigo, K.R., Lubin, D., van Dijken, G.L., Holm-Hansen, O., Morrow, E., 2003. Impact of a deep ozone hole on southern ocean primary production. Journal of Geophysical Research 108, 3154.

Arrigo, K.R., Robinson, D.H., Worthen, D.L., Schieber, B., Lizotte, M.P., 1998. Bio-optical properties of the southwestern Ross Sea. Journal of Geophysical Research 103, 21683–21695.

Arrigo, K.R., Sullivan, C.W., Kremer, J.N., 1991. A bio-optical model of Antarctic sea ice. Journal of Geophysical Research 96, 10581–10592.

Dieckmann, G.S., Eicken, H., Haas, C., Garrison, D.L., Gleitz, M., Lange, M., Nothig, E.-M., Spindler, M., Sullivan, C.W., Thomas, D.N., Weissenberger, J., 1998. A compilation of data on sea ice algal standing crop from the Bellingshausen, Amundsen and Weddell Seas from 1983 to 1994. In: Lizotte, M.P., Arrigo, K. (Eds.), Antarctic Sea Ice Biological Processes, Interactions, and Variability. American Geophysical Union, Washington, DC, pp. 85–92.

Eicken, H., Lange, M.A., Dieckmann, G.S., 1991. Spatial variability of sea-ice properties in the northwestern Weddell Sea. Journal of Geophysical Research 96, 10603–10615.

Ferrari, G.M., Tassan, S., 1996. Use of the 0.22 um Millipore membrane for light-transmission measurements of aquatic particles. Journal of Plankton Research 18, 1261–1267.

Fritsen, C.H., Coale, S.L., Neenan, D.R., Gibson, A.H., Garrison, D.L., 2001. Biomass, production and microhabitat characteristics near the freeboard of ice floes in the Ross Sea, Antarctica, during the austral summer. In: Jeffries, M.O., Eicken, H. (Eds.), Annals of Glaciology. International Glaciological Society, Cambridge, pp. 280–286.

Fritsen, C.H., Iturriaga, R., Sullivan, C.W., 1992. Influence of particulate matter on spectral irradiance fields and energy transfer in the Eastern Arctic Ocean. Ocean Optics XI 1750, 527–541.

Fritsen, C.H., Memmott, J., Stewart, F.J., 2008. Inter-annual sea-ice dynamics and micro-algal biomass in winter pack ice of Marguerite Bay, Antarctica. Deep Sea Research II 55, 2059–2067.

Fritsen, C.H., Sullivan, C.W., 1997. Distributions and dynamics of microbial communities in the pack ice of the western Weddell Sea, Antartica. In: Battaglia, B., Valencia, J., Walton, D.W.H. (Eds.), Antarctic communities: species, structure, and survival. Cambridge University Press, Cambridge, pp. 101–106.

Fritsen, C.H., Sullivan, C.W., 1999. Distributions and dynamics of microbial communities in the pack ice of the western Weddell Sea, Antarctica. Biology Symposium, 1-20.

Garrison, D.L., Buck, K.R., 1986. Organism losses during ice melting: a serious bias in sea ice community studies. Polar Biology 6, 237–239.

Garrison, D.L., Gibson, A., Coale, S.L., Gowing, M.M., Okolodkov, Y.B., Fritsen, C.H., Jeffries, M.O., 2005. Sea-ice microbial communities in the Ross Sea: autumn and summer biota. Marine Ecology-Progress Series 300, 39–52.

Garrison, D.L., Sullivan, C.W., Ackley, S.F., 1986. Sea ice microbial communities in Antarctica. BioScience 36, 243–250.

Grenfell, T.C., 1983. A theoretical model of the optical properties of sea ice in the visible and near infrared. Journal of Geophysical Research 88, 9723–9735.

Grossi, S., Kottmeier, S.T., Moe, R.L., Taylor, G.T., Sullivan, C.W., 1987. Sea ice microbial communities. VI. Growth and primary production in bottom ice under graded snow cover. Marine Ecology 35, 153–164.

Grossi, S.M., Kottmeier, S.T., Sullivan, C.W., 1984. Sea ice microbial communities. III. Seasonal abundance of microalgae and associated bacteria, McMurdo Sound, Antarctica. Microb Ecology 10, 231–242.

Hillebrand, H., Durselen, C.-D., Kirschtel, D., Pollingher, U., Zohary, T., 1999. Biovolume calculation for pelagic and benthic microalgae. Journal of Phycology 35, 403–424.

Horner, R.A., 1980. Ecology and productivity of Arctic Sea ice diatoms. 6th Diatom-Symposium, 359–369.

Jeffrey, S.W., MacTavish, H.S., Dunlap, W.C., Vesk, M., Groenewoud, K., 1999. Occurrence of UVA- and UVB-absorbing compounds in 152 species (206 strains) of marine microalgae. Marine Ecology-Progress Series 189, 35–51.

Johnson, M.D., Tengs, T., Oldach, D., Stoecker, D.K., 2006. Sequestration, performance, and functional control of cryptophyte plastids in the ciliate Myrionecta rubra (Ciliophora). Journal of Phycology 42, 1235–1246.

Karentz, D., 1991. Ecological considerations of Antarctic ozone depletion. Antartic Science 3, 3–11.

Karentz, D., 1994. Ultraviolet tolerance mechanisms in Antarctic marine organisms. In: Weiler, C.S., Penhale, P.A. (Eds.), Ultraviolet Radiation in Antarctica: Measurement and Biological Effects. American Geophysical Union, Washington D.C.

Kirk, J.T.O., 1996. Light and photosynthesis in aquatic ecosystems.. Cambridge University Press, New York.

Kishino, M., Takahashi, M., Okami, N., Ichimura, S., 1985. Estimation of the spectral absorption coefficients of phytoplankton in the sea. Bulletin of Marine Science 37, 634–642.

Lewis, M.J., Tison, J.L., Weissling, B., Delille, B., Ackley, S.F., Brabant, F., Xie, H., 2011. Sea ice and snow cover characteristics during the winter-spring transition in the Bellingshausen Sea: an overview of SIMBA 2007. Deep Sea Research II 58 (9–10), 1019–1038.

Meguro, H., 1962. Plankton ice in the Antarctic ocean. Report of the Japanese Antarctic Research Expedition, 1192–1199.

Moisan, T.A., Mitchell, B.G., 2001. UV absorption by mycosporine-like amino acids in *Phaeocystis antarctica* Karsten induced by photosynthetically available radiation. Marine Biology 138, 217–227.

Mundy, C.J., Barber, D.G., Michel, C., 2005. Variability of snow and ice thermal, physical and optical properties pertinent to sea ice algae biomass during spring. Journal of Marine Systems 58, 107–120.

Mundy, C.J., Ehn, J.K., Barber, D.G., Michel, C., 2007. Influence of snow cover and algae on the spectral dependence of transmitted irradiance through Arctic landfast first-year sea ice. Journal of Geophysical Research-Oceans, 112.

Neale, P.J., Banaszak, A.T., Jarriel, C.R., 1998. Ultraviolet sunscreens in *Gymnodinium sanguineum* (Dinophyceae): Mycosporine-like amino acids protect against inhibition of photosynthesis. Journal of Phycology 34, 928–938.

Norman, L., Thomas, D.N., Stedmon, C.A., Granskog, M.A., Papadimitriou, S., Meiners, K.M., Lannuzel, D., van der Merwe, P., Dieckmann, G.S., 2011. The characteristics of dissolved organic matter (DOM) and chromophoric dissolved organic matter (CDOM) in Antarctic sea ice. Deep Sea Research II 58 (9–10), 1075–1091.

Palmisano, A.C., Kottmeier, S.T., Moe, R.L., Sullivan, C.W., 1985. Sea ice microbial communities. IV. The effect of light perturbation on microalgae at the ice-seawater interface in McMurdo Sound, Antartica. Marine Ecology Progress Series 21, 37–45.

Palmisano, A.C., SooHoo, J.B., Moe, R.L., Sullivan, C.W., 1987. Sea ice microbial communities. VII. Changes in under-ice spectral irradiance during the development of Antarctic sea ice microalgal communities. Marine Ecology Progress Series 35, 165–173.

Perovich, D.K., 1989. A two-stream multilayer, spectral radiative transfer model for sea ice. U.S. Army Cold Regions Research and Engineering Laboratory Report CR89-15, pp. 1–17.

Perovich, D.K., 1990. Theoretical estimates of light reflection and transmission by spatially complex and temporally varying sea ice covers. Journal of Geophysical Research 95, 9557–9567.

Perovich, D.K., 1993. A theoretical model of ultraviolet light transmission through Antarctic Sea ice. Journal of Geophysical Research 98, 22579–22587.

Perovich, D.K., Cota, G.F., Maykut, A., Grenfell, T.C., 1993. Bio-optical observations of first-year Arctic Sea Ice. Geophysical Research Letters 20, 1059–1062.

Perovich, D.K., Grenfell, T.C., 1982. A theoretical model of radiative transfer in young sea ice. Journal of Glaciology 28, 320–341.

Perovich, D.K., Maykut, G.A., Grenfell, T.C., 1986. Optical properties of ice and snow in the polar oceans. I: observations. SPIE Ocean Optics VIII 637, 232–241.

Ryan, K.G., McMinn, A., Mitchell, K.A., Trenerry, L., 2002. Mycosporine-like amino acids in Antarctic sea ice algae, and their response to UVB radiation. Z. Naturforschung 57, 471–477.

Smith, R.C., Prezelin, B.B., Baker, K.S., Bidigare, R.R., Boucher, N.P., Coley, T., Karentz, D., MacIntyre, S., Matlick, H.A., Menzies, D., Ondrusek, M., Wan, Z., Waters, K.J., 1992. Ozone depletion: ultraviolet radiation and phytoplankton biology in antarctic waters. Science 255, 952–958.

Smith, R.E.H., Anning, J., Clement, P., Cota, G., 1988. Abundance and production of ice algae in Resolute Passage, Canadian Arctic. Marine Ecology Progress Series 48, 251–263.

Stoecker, D.K., Buck, K.R., Putt, M., 1992. Changes in the sea-ice brine community during the spring-summer transition, McMurdo Sound, Antarctica. I. Photosynthetic protists. Marine Ecology Progress Series 84, 265–278.

Stoecker, D.K., Gustafson, D.E., Black, M.M.D., Baier, C.T., 1998. Population dynamics of microalgae in the upper land-fast sea ice at a snow-free location. Journal of Phycology 34, 60–69.

Stoecker, D.K., Gustafson, D.E., Merrell, J.R., Black, M.M.D., Baier, C.T., 1997. Excystment and growth of chrysophytes and dinoflagellates at low temperatures and high salinities in Antarctic sea-ice. Journal of Phycology 33, 585–595.

Tassan, S., Ferrari, G.M., 1995. An alternative approach to absorption measurements of aquatic particles retained on filters. Limnology and Oceanography 40, 1358–1368.

Thomas, D.N., Dieckmann, G.S., 2002. Biogeochemistry of Antarctic Sea Ice. Oceanography and Marine Biology: an Annual Review 40, 143–169.

Warren, S.G., 1982. Optical properties of snow. Reviews of Geophysics and Space Physics 20, 67–89.

Zeebe, R.E., Eicken, H., Robinson, D.H., Wolf-Gladrow, D., Dieckmann, G.S., 1996. Modeling the heating and melting of sea ice through light absorption by microalgae. Journal of Geophysical Research 101, 1163–1181.